Journal of The Electrochemical Society, **147** (12) 4524-4535 (2000)
S0013-4651(00)04-078-7 CCC: $7.00 © The Electrochemical Society, Inc.

Superconformal Electrodeposition of Copper in 500-90 nm Features

T. P. Moffat,[a,*,z] J. E. Bonevich,[a] W. H. Huber,[b] A. Stanishevsky,[c] D. R. Kelly,[a] G. R. Stafford,[a,*] and D. Josell[a]

[a]*Materials Science and Engineering Laboratory and* [b]*Electrical and Electronic Engineering Laboratory, National Institute of Standards and Technology, Gaithersburg, Maryland 20899, USA*
[c]*Institute for Plasma Research, Department of Physics, University of Maryland, College Park, Maryland 20742, USA*

Superconformal electrodeposition of copper in 500 nm deep trenches ranging from 500 to 90 nm in width has been demonstrated using an acid cupric sulfate electrolyte containing chloride (Cl), polyethylene glycol (PEG), and 3-mercapto-1-propanesulfonate (MPSA). In contrast, similar experiments using either an additive-free electrolyte, or an electrolyte containing the binary combinations Cl-PEG, Cl-MPSA, or simply benzotriazole (BTAH), resulted in the formation of a continuous void within the center of the trench. Void formation in the latter electrolytes is shown to be reduced through the geometrical leveling effect associated with conformal deposition in trenches or vias with sloping sidewalls. The slanted sidewalls also counterbalance the influence of the differential cupric ion concentration that develops within the trenches. Examination of the *i-E* deposition characteristics of the electrolytes reveals a hysteretic response associated with the Cl-PEG-MPSA electrolyte that can be usefully employed to monitor and explore additive efficacy and consumption. Likewise, resistivity measurements performed on corresponding blanket films can be used to quantify the extent of additive incorporation and its influence on microstructural evolution. The films deposited from the Cl-PEG-MPSA electrolyte exhibit spontaneous recrystallization at room temperature that results in a 23% drop in resistivity within a few hours of deposition.
© 2000 The Electrochemical Society. S0013-4651(00)04-078-7. All rights reserved.

Manuscript submitted April 24, 2000; revised manuscript received August 9, 2000.

The successful implementation of copper electroplating technology in the metallization of electronic devices derives from the use of electrolyte additives to affect the local deposition rate, thereby allowing superconformal or "superfilling" of trenches and vias in the Damascene process.[1] The first description of this process was adopted from the theory of additive-induced leveling whereby the electrolyte additive(s) adsorb at the metal electrolyte interface, reducing the active area and thereby inhibiting the metal reduction process.[1,2] Since the inhibitor concentration is dilute (10^{-3} to 10^{-6} mol/L) the adsorption process is typically considered to be diffusion limited while the copper deposition process proceeds under interfacial charge-transfer control. In order to maintain transport control of the inhibitor flux, the adsorbate must either be incorporated in the growing film or undergo reductive desorption during metal deposition. For the Damascene process, the trench or via geometry results in a lower flux of the inhibitor to the bottom of the features than to the external surface. Consequently, the metal deposition kinetics proceed more rapidly at the bottom of the trench which results in superconformal filling. This model also predicts that the slowest growth occurs at the edge demarcating the entrance of the trench or via where the inhibitor flux is expected to be greatest.[3] However, it was necessary to empirically modify the simple area-blockage leveling theory in order to capture the experimentally observed corner rounding and general shape change behavior.[1] The complexity of additive-electrode interactions was recently highlighted by the observation of "overfill" where the originally concave surface profile becomes convex due to a sustained differential rate of metal deposition that cannot be rationalized by the transport-limited inhibition model outlined here.[4-6] Rather, this observation has focused attention on the competition between species that accelerate *vs.* suppress deposition in the multicomponent additive packages, thereby demonstrating the need for detailed information concerning the surface chemistry of copper in solutions containing additives.

In addition to influencing the kinetics of metal reduction, electrolyte additives are also known to exert a dramatic effect on the metallurgical microstructure. Specifically, certain additives sharply inhibit epitaxial growth, leading to fine-grained deposits and incorporation of the additives and/or the corresponding breakdown products as impurities within the film.[7-9] In certain instances, the physical defects and light element impurities lead to room temperature recrystallization within a few hours of deposition. This relaxation is typically accompanied by a beneficial reduction in the electrical resistivity of the deposits.[7,10]

One of the difficulties associated with studying superconformal electrodeposition has been the proprietary nature of the processing parameters employed throughout the industry. Nonetheless, a brief survey of the literature suggests that electrolyte formulations that have previously been used for plating throughholes in printed circuit boards may be an effective starting point for exploring submicrometer superconformal deposition.[11-15] The first complete report of the chemistry and processing conditions used to demonstrate "superfill" in submicrometer dimensions was recently published based on the polyether, thiol, chloride, and diethyl safranine azo dimethyl aniline (Janus Green B) chemistry[16] that stems from the patent literature.[17] The films were deposited galvanostatically under quiescent conditions. The most effective superfilling under these conditions required the use of all four additives that resulted in the filling of 90% of the trenches examined. In contrast, an electrolyte closely related to that used in this study reportedly filled only 50% of the trenches.

In this paper superconformal deposition over a wide range of feature sizes and aspect ratios is demonstrated using a polyether (polyethylene glycol, PEG), thiol (3-mercapto-1-propanesulfonate, MPSA), and chloride (Cl) electrolyte. Complete filling was observed for films grown potentiostatically in a regime corresponding to mixed kinetic/diffusion control for copper deposition. For control purposes, deposition from an additive-free electrolyte was also investigated. Additional experiments with various combinations of Cl-PEG-MPSA as well as experiments with the sole addition of benzotriazole (BTAH) were performed in an attempt to assess the possibility of correlating simple *i-E* measurements of inhibition with superconformal deposition. BTAH, which is widely used as a corrosion inhibitor,[18] is also known to inhibit copper deposition and yield bright deposits,[19-21] thereby enabling the effect of surface roughness on feature filling to be explored. Furthermore, analysis of electrodeposits revealed that the incorporated BTAH molecule could be recovered in the native form, which suggests that this electrolyte might be an ideal agent for examining inhibition and additive incorporation effects.[19] These experiments were complemented by resistivity measurements of blanket films that provide a preliminary assessment of the extent of additive incorporation through its influence on metallurgical structure.

* Electrochemical Society Active Member.
[z] E-mail: tmoffat@nist.gov

S0013-4651(00)04-078-7 CCC: $7.00 © The Electrochemical Society, Inc.

Experimental

Specimen fabrication for trench filling experiments.—Copper was electrodeposited onto patterned polymethylmethacrylate (PMMA)/Si substrates that had been coated with a copper seed layer. The patterning of the PMMA was accomplished using electron-beam lithography. The polymer was spincoated onto Si wafers to approximately 500 nm thickness (height) followed by annealing at 440 K. The individual lines were created using the electron-beam of a scanning electron microscope (SEM) to write the pattern on the PMMA followed by immersion in a 1:3 solution of isopropyl alcohol:methyl isobutyl ketone for 2 min to dissolve the exposed material. The thinnest lines were fabricated using a single line dose while the thicker lines were formed using overlapping, adjacent line doses. As fabricated, the unfilled trenches had PMMA sidewalls and a Si, with native oxide, base as verified by SEM. Two different trench arrangements were examined. In the first series of experiments, groups of six 250 μm long lines, running in parallel 2 μm apart (center to center) and ranging in width from approximately 100 to 500 nm, were the basic lithographic repeat unit. Each electrodeposition specimen consisted of six such groups, spaced approximately 30 μm apart and covering a total area of 250 × 250 μm. Examination of specimens revealed significant distortion of the trenches due to stresses that develop during seed-layer deposition. Typically, the deformation resulted in sidewall angles deviating approximately 5-7° from the vertical axis. As shown later, the deviation was usefully employed to examine the effects of slanted sidewalls on trench filling by electrodeposition. In the second series of experiments, pattern distortion was minimized by lowering the trench spacing to approximately 0.5 μm and by placing sacrificial trenches along the sides of each group of lines and around the periphery of the patterned region. This effectively isolated the patterned trenches from the surrounding stress fields generated during seed-layer deposition. Two more groups of lines were added, making for a total of eight per specimen, and the trench lengths were shortened to 100 μm (for convenience).

The copper seed layer was deposited on the patterned PMMA (including bottom, sidewalls, and upper surface) by electron-beam evaporation in a deposition system with base vacuum of 1×10^{-6} Pa (1×10^{-8} Torr). The pressure rose over two orders of magnitude at the start of deposition as chamber bakeout was avoided to minimize the already mentioned warping of the trenches. The patterned substrates were mounted on a water-cooled, tilting stage during deposition. The trenches were oriented parallel to the tilt axis so that Cu could be deposited on the sidewalls. The seed layer was deposited with the atomic flux arriving symmetrically over the angular range of −10 to +10° from the substrate normal. This 20° range was selected to yield adequate thickness of Cu deposited on the sidewalls while ensuring continuity at the corners where the PMMA sidewalls meet the Si bottom. Note that for the trenches with the highest aspect ratio (~5.5:1 height to width), the maximum angle for which the incoming flux can reach these corners is approximately 9.6°. A variety of seed-layer thicknesses were examined, ranging from 40 to 110 nm on the top surface. The 110 nm thick seed layers were found to be the most reliable and were used for most of the samples described in this paper. The nominal seed-layer thickness of 110 ± 5 nm corresponded to 6 ± 0.5 nm on each of the (vertical) sidewalls for the tilt angles used. Because the trench depths at the start of electrodeposition were unchanged by deposition of the seed layer while the widths decreased by approximately 12 nm, the effective aspect ratios of the trenches were slightly higher than the PMMA defined aspect ratios.

Specimen analysis.—A series of electrodeposition experiments were performed where all six or eight groups of Cu-seeded trenches on each specimen were simultaneously exposed to a particular bath and processing parameters. The films were grown to an average thickness ranging from ~200 to 500 nm. Cross sections of some specimens were viewed by SEM. Such specimens were prepared by gluing a glass cover slip to the Cu surface followed by grinding, mechanical polishing (to 0.05 μm diamond finish), and ion milling (using argon ions to remove the mechanically damaged region). In order to assay the defect population, such as voids in the trenches, views at multiple locations along the lines were examined by repetitive ion milling. In other experiments, a focused ion beam microscope (FIB) using a liquid gallium ion source was utilized to mill and image cross sections of the trenches. In addition to ease of specimen preparation, the FIB reveals grain structure due to modulation of the secondary electron yield as a result of crystallographic channeling of the probing ions. The ion source was first used to mill a trench perpendicular to the lithographically defined trenches. The high ion flux (and/or beam energy) used for this milling step led to significant warping of the PMMA template so a period of ion-beam polishing was used to remove these artifacts. The FIB images were collected with the normal of the viewed cross section tilted 30° from the incoming gallium beam; thus, the trench depths appear compressed by 15% in the images. However, imaging of the lateral dimensions is unaffected by the geometry, so the fiduciary marker shown in the FIB images corresponds to the correct lateral length scale.

Electrodeposition.—Six different electrolytes were used in this study, as shown in Table I. The basic electrolyte was 0.25 mol/L $CuSO_4$ and 1.8 mol/L H_2SO_4 to which a combination of 1.0×10^{-3} mol/L NaCl (Cl), 1×10^{-5} mol/L $NaSO_3(CH_2)_3SH$ (sodium MPSA), and/or 8.8×10^{-5} mol/L $H(OCH_2CH_2)_{55}OH$ (PEG, average molar mass ~3400 g/mol), was added. The effect of the sole addition of the corrosion inhibitor BTAH was also examined for two different concentrations. In the highly acidic cupric sulfate solution, BTAH is known to be protonated to $BTAH_2^+$.[18] However, for simplicity, the molecules are referred to as in its native form, BTAH, for the remainder of the paper. A standard three-electrode cell with a copper counter electrode and a saturated mercurous sulfate electrode (SSE) was used for all measurements. Care was taken to ensure that the position of the working electrode was held constant relative to the reference electrode in order to minimize variation in the iR drop between experiments. The electrochemical characteristics of the various electrolytes were established using a polished copper working electrode (area 2.755 cm^2) to 1200 grade SiC. All experiments were performed under quiescent conditions. Copper was deposited on the patterned wafers using a masked copper alligator clip as the contact. The nominal geometric electrode area ranged between 1.5 and 2.5 cm^2. The poor adhesion of evaporated copper to PMMA, which often resulted in partial peeling of the seed layer, was a significant difficulty in this study. The strain relief channels around the perimeter of the area of interest were effective in preventing decohesion in this region. However, in certain instances much of the surrounding

Table I. Electrolyte composition (mol/L).

Name	$CuSO_4 \cdot 5H_2O$	H_2SO_4	Cl^-	PEG (3400 Mw)	MPSA	BTAH
Additive-free	0.25	1.8				
CI-PEG	0.25	1.8	1×10^{-3}	88.2×10^{-6}		
CI-MPSA	0.25	1.8	1×10^{-3}		1×10^{-5}	
CI-PEG-MPSA	0.25	1.8	1×10^{-3}	88.2×10^{-6}	1×10^{-5}	
BTAH	0.25	1.8				1×10^{-5}
BTAH	0.25	1.8				1×10^{-4}

S0013-4651(00)04-078-7 CCC: $7.00 © The Electrochemical Society, Inc.

area was disturbed, making measurement of the actual electroactive area difficult. In light of this uncertainty, the wafers were plated under potentiostatic conditions that correspond to the steady-state potentials observed for blanket films grown galvanostatically at 15 mA/cm^2.

Resistivity experiments.—The influence of additive chemistry on impurity incorporation and microstructural evolution, *e.g.,* recrystallization, was examined on copper films that were electrodeposited onto copper seed layers deposited on silicon (100) wafers. The silicon substrates were first sputter cleaned, followed by evaporation of 3.0 nm adhesion-promoting layers of chromium and 100 nm seed layers of copper. The seed layers were polycrystalline with a slight (111) preferred orientation. For electroplating, the silicon wafers were supported on a copper plate with an ohmic contact being formed using a liquid gallium-indium alloy corresponding to the eutectic composition. The wafer and copper current collector were masked with electroplater's tape. A 2.54 cm diam hole exposed 5.1 cm^2 of the copper seed layer to the electrolyte. The counter electrode was a flat platinum sheet placed parallel to and positioned laterally 8 cm from the working electrode. The electrolytes (1 L) were used shortly after preparation and the total electrolysis times were only 3 min to minimize any bath aging effects associated with oxidation at the platinum anode. Electrodeposition was conducted at room temperature. The copper films were electrodeposited under quiescent conditions at a current density of 15 mA/cm^2 yielding a total film thickness of 1 μm. Immediately after rinsing, the freshly deposited samples were examined by a four-point resistance probe. Films were maintained at room temperature during the characterization period.

Results

i-E Characteristics.—The steady-state *i-E* characteristics for copper deposition from electrolytes containing various combinations of Cl-PEG-MPSA are shown in Fig. 1. In agreement with previous reports, the addition of Cl-PEG[12,22-27] provides significant inhibition of the deposition reaction while the combination of Cl-MPSA leads to an acceleration of the deposition rate.[11,14] The combined action of all three additives, Cl-PEG-MPSA, yields net inhibition relative to additive-free electrolyte, although an acceleration of the rate relative to the Cl-PEG electrolyte is apparent, which reflects the competition between the effects of PEG and MPSA. At high overpotentials a diffusion-limited current, i_L, of ~20 mA/cm^2 is observed. This corresponds to a nominal boundary layer thickness of ~120 μm that is established by convection due to the cupric ion density gradient in the otherwise quiescent solution.[28] For comparison purposes, the free convection boundary layer in these experiments roughly corresponds to a rotation rate of 70 rpm for a rotating disk electrode. Thus, deposition from a quiescent electrolyte of concentration c_{bulk} at the industrially relevant rates of 5-15 mA/cm^2 results in significant cupric ion depletion at the planar interface, $c_{x=0}$, according to the expression

$$\frac{c_{x=0}}{c_{\text{bulk}}} = 1 - \frac{i}{i_L}$$

This is in contrast to the assumption $c_{x=0} = c_{\text{bulk}}$ used in many existing models of superconformal deposition. Most of the films examined in this study were grown under conditions corresponding to a steady-state deposition rate of 15 mA/cm^2, *i.e.,* $c_{x=0} = 0.25C_{\text{bulk}}$, indicating that significant copper depletion occurs during film growth. Although the central issue remains the differential concentration that develops between the trench bottom and the free surface, quantitative models should be adjusted to reflect the effects of cupric ion depletion. Another important consequence of operating under mixed control is that the approach to the steady-state conditions will depend significantly on whether galvanostatic or potentiostatic regulation is used. In the case of galvanostatic control from an additive-free electrolyte, as shown in Fig. 2, a current density of ~15 mA/cm^2 results in the potential slowly decreasing over a period of approximately 60 s toward a steady-state value of −0.570 V. In contrast, potential step experiments initially generate a much higher current density. Because this cannot be sustained by cupric ion diffusion, a $t^{-1/2}$ decay results as the concentration gradient decreases to a steady-state value defined by free convection. As shown in Fig. 3, a potential step from the open-circuit potential to −0.572 V results in an initial current density of ~55 mA/cm^2 that decays within 30 s to a steady-state value of ~15 mA/cm^2. The corresponding film thickness obtained by integration is plotted relative to that for galvanostatic deposition in Fig. 4. This figure provides an estimate of the time required to fill a given trench if growth is conformal. For example, a 200 nm wide square trench would be considered filled when the film thickness on the free surface equals half the trench width, *i.e.,* at a film thickness of 100 nm. For the conditions outlined in Fig. 4 ($E = -0.572$ V), a 200 nm wide trench would be filled in less than 8.5 s while galvanostatic deposition would require twice as long. Based on this simple calculation and Fig. 3, filling of the trenches of interest occurs within the period of the transient for these processing conditions. The distinction between potentiostatic and galvanostatic regulation is expected to become increasingly important when the additive adsorption and consumption dynamics are a strong function of the metal deposition flux (potentiostatic condition) or overpotential (galvanostatic condition).

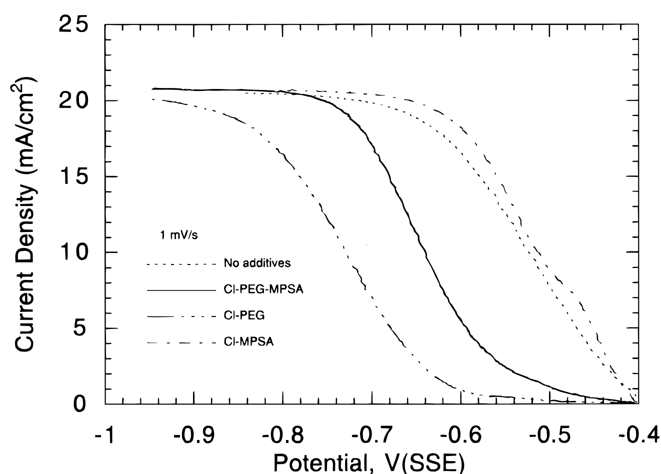

Figure 1. The steady-state *i-E* characteristics for copper deposition from the various electrolytes given in Table I. The Cl-PEG electrolyte yields inhibition of the deposition reaction while Cl-MPSA system leads to an acceleration of the deposition rate. The combination of all three additives indicates a competition between these two effects that results in net inhibition relative to deposition from the additive-free solution.

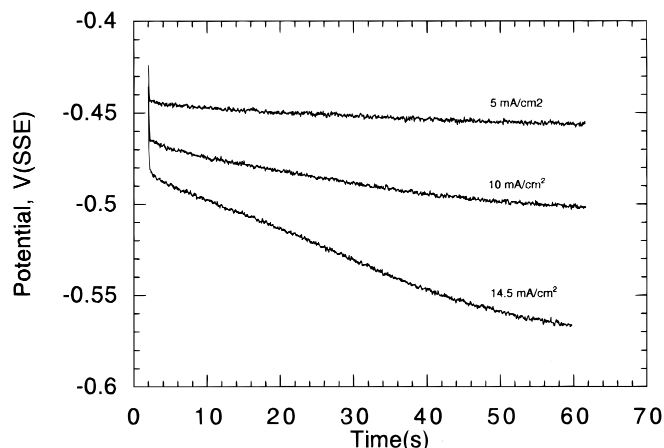

Figure 2. Potential transients for galvanostatic deposition at various current densities from the additive-free electrolyte.

S0013-4651(00)04-078-7 CCC: $7.00 © The Electrochemical Society, Inc.

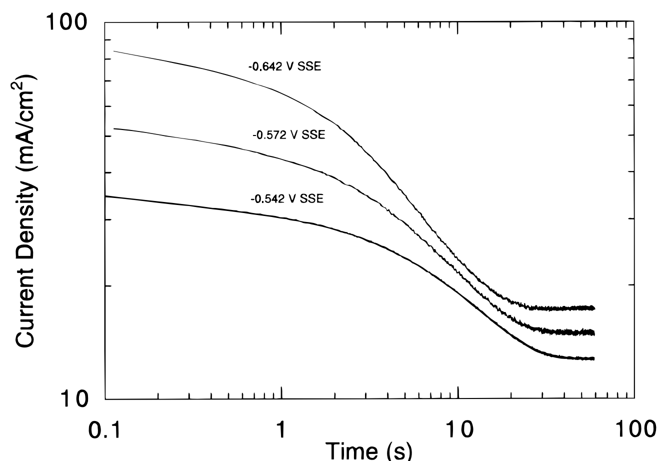

Figure 3. A series of chronoamperometric transients for deposition at various potentials from the additive-free electrolyte. The early time response correspond to growth being determined by the rate of charge transfer. Growth is subsequently constrained by diffusion, resulting in the $t^{-1/2}$ decay toward the steady-state value determined by free convection.

As noted earlier, in conventional models of leveling, diffusion-limited adsorption of the inhibiting additives is invoked. For transport control to be sustained, two limiting possibilities exist.[2,29] Either the additive is consumed by reduction and subsequent desorption or the molecule is incorporated in the growing electrodeposit. In the case of the reductive desorption, the rate is expected to be directly dependent on the electrode potential; while in the case of incorporation the rate of metal deposition relative to the rate of additive desorption is the important parameter. It is also possible for an additive system to exhibit a combination of these two effects, particularly in multicomponent additive packages. One important consequence of the competition between these various processes is the possibility of hysteresis in the voltammetric behavior.[4,29] As shown in Fig. 5, significant hysteresis is apparent in the case of Cl-PEG-MPSA electrolyte, although little or no hysteresis is observed for the binary combinations Cl-PEG, Cl-MPSA, or the additive-free electrolyte. The lack of hysteresis of the Cl-PEG and Cl-MPSA electrolytes indicates that no irreversible changes of the surface chemistry occur as the metal deposition flux ratio i/i_L ranges from 0 to 1. In contrast, the hysteresis associated with the full combination of additives indicates that the competition between inhibition provided by the Cl-PEG $Cu^{2+}/Cu^{+}/Cu$ interaction and the catalytic effects of Cl-MPSA/$Cu^{2+}/Cu^{+}/Cu$ interaction leads to an irreversible change in the reaction dynamics. The extent of the hysteresis scales with the negative limit of the potential sweep as shown in Fig. 6. Increasing the MPSA concentration leads to a decrease in the area enclosed by the hysteresis loop and displacement of the *i-E* curve toward the Cl-MPSA curve, *i.e.,* toward positive potentials, as indicated in Fig. 7.

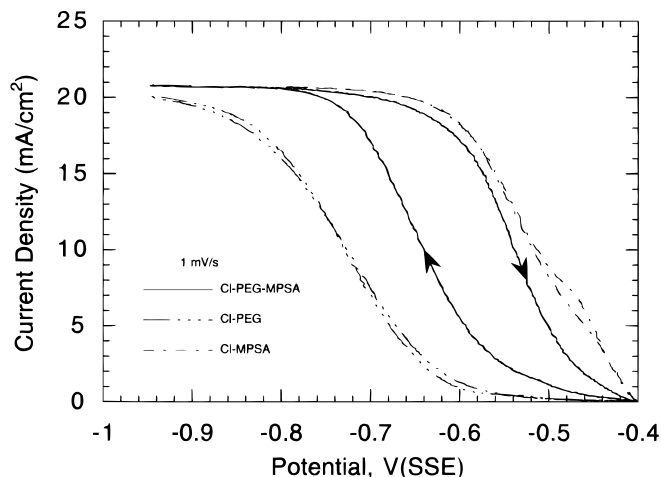

Figure 5. A distinct hysteresis loop is observed in the *i-E* curve for Cl-PEG-MPSA electrolyte that is absent for the binary additive combinations.

In an attempt to simplify the process, the efficacy of a single additive system was explored. BTAH, a well-known corrosion inhibitor, has been shown to be an effective brightener,[19,21] although its possible role as a leveling agent does not appear to have been examined. As shown in Fig. 8, the extent of inhibition scales with the BTAH concentration. A concentration-dependent wave is apparent at low overpotentials. The strong interaction between cuprous ions and BTAH and its derivatives is well known and may play a role in the observed inhibition.[19] Likewise, the formation of ordered two-dimensional BTAH domains on copper surfaces at negative potentials has been examined by scanning tunneling microscopy (STM)[30,31] and vibrational spectroscopy.[32] In contrast to the Cl-PEG-MPSA electrolyte, only minor hysteresis is observed during the return sweep, although the small wave at low overpotentials is no longer apparent.

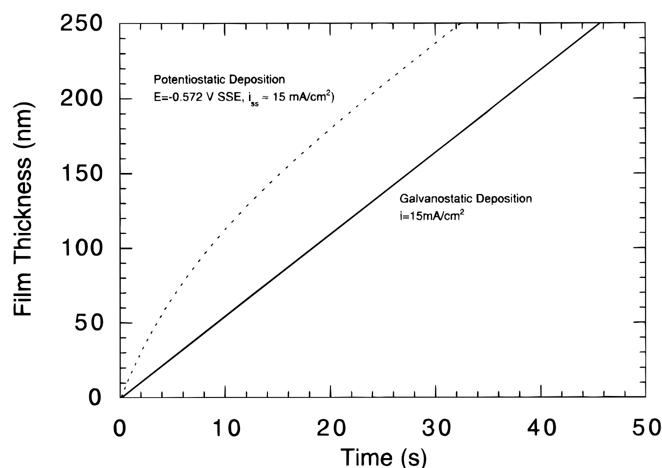

Figure 4. The effect of regulation mode on the rate of film growth. By assuming conformal growth the time required to fill a trench can be estimated as the time required to reach a film thickness equivalent to half the trench width. For the potentiostatic condition used in this study a 180 nm trench would be filled in 8 s while filling by the galvanostatic process would require 17 s.

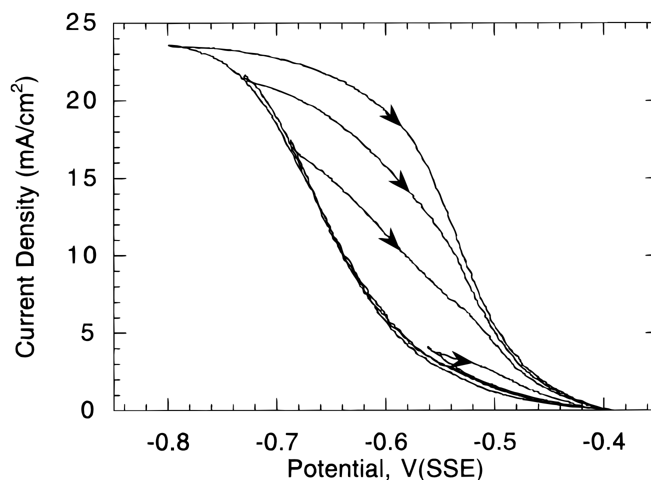

Figure 6. The extent of the hysteresis loop is a strong function of the negative limit of the linear potential scan. This reflects the convolution of potential-dependent changes in surface chemistry with the renewal of the surface. The latter occurs with increasing rate as the potential is swept in the negative direction.

Journal of The Electrochemical Society, **147** (12) 4524-4535 (2000)
S0013-4651(00)04-078-7 CCC: $7.00 © The Electrochemical Society, Inc.

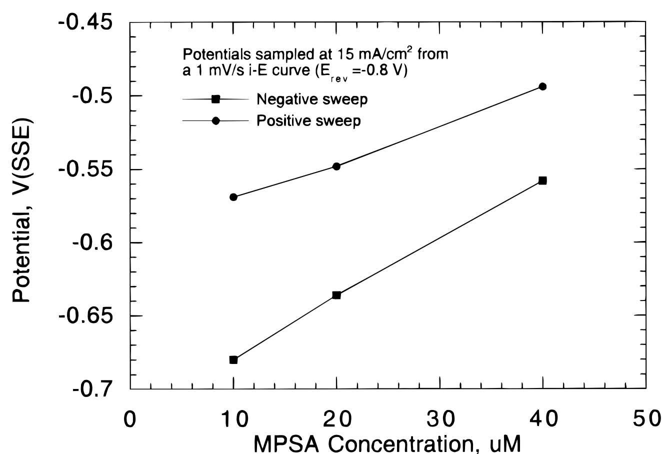

Figure 7. The shape and polarization of the hysteresis loop is a function of the MPSA concentration. This effect could be used as process control parameter.

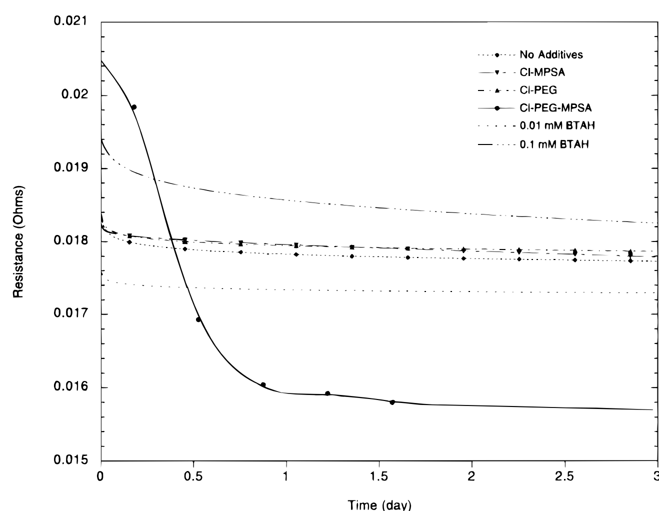

Figure 9. Resistance transients during aging of 1 μm thick films at room temperature. The distinct influence of the synergistic interaction between the constituents of the Cl-PEG-MPSA additives is apparent.

Resistivity measurements.—Electroplated copper films typically have a much higher electrical resistivity than bulk copper. The excess resistivity is associated with the defect structure in the electrodeposited films and is the result of scattering from grain boundaries, dislocations, vacancies, impurity atoms in solution, as well as second-phase particles.[7] The electrical resistance of thin blanket films was used to probe the influence of additive chemistry on impurity incorporation and its effect on microstructural evolution. The temporal evolution of the sheet resistance of 1 μm thick copper films, electrodeposited from the copper sulfate–sulfuric acid electrolyte containing the various addition agents, is summarized in Fig. 9. The films were deposited under galvanostatic control; however, the transient period described earlier for potentiostatically deposited films corresponds only to ~10% of the film thickness. Thus, the regulation mode is not expected to strongly perturb the value of the initial resistance, although the nucleation of subsequent microstructural relaxations might be affected. Copper films electrodeposited from electrolytes containing no additives, Cl-PEG, and Cl-MPSA showed nearly identical resistance-time behavior during the first 72 h after deposition. The resistance decreased by less than 3% over this period. In sharp contrast, copper films electrodeposited from electrolytes containing Cl-PEG-MPSA had an initial resistance that was 12% higher than the other films but decreased by 23% within 24 h. An X-ray diffraction (XRD) study of these films revealed that a significant fraction of the resistance drop was due to recrystallization and grain growth that resulted in a reduced grain-boundary density.[33] This finding is in excellent agreement with results reported for films deposited from proprietary electrolytes by several industrial concerns.[7,10]

Examination of the initial film resistances shown in Fig. 9 provides some insight into the extent of additive incorporation and the effectiveness of the various agents with regards to grain refinement. The minor alterations of the initial resistance induced by Cl-PEG and Cl-MPSA reflects minimal perturbations of the microstructure that are in sharp contrast to the effects induced by the combination Cl-PEG-MPSA. The changes in the latter case are a direct indication of additive incorporation and grain refinement. Thus, resistivity data provide another measure of the synergism that exists between the constituents of the Cl-PEG-MPSA electrolyte. This observation also supports the attribution of the hysteresis in the i-V curves to additive incorporation and the coincident alteration of the surface structure and reaction dynamics.

The resistivities of two films grown in the presence of BTAH are also shown in Fig. 9. Films grown in solution with less than 20 μM BTAH exhibited resistance values analogous to the additive-free, Cl-PEG, and Cl-MPSA electrolytes. However, the surface finish became increasingly specular and, as shown in Fig. 10, the value of the initial resistance increased rapidly with increasing BTAH concentration. Above a concentration of 1 mM BTAH it was visually apparent

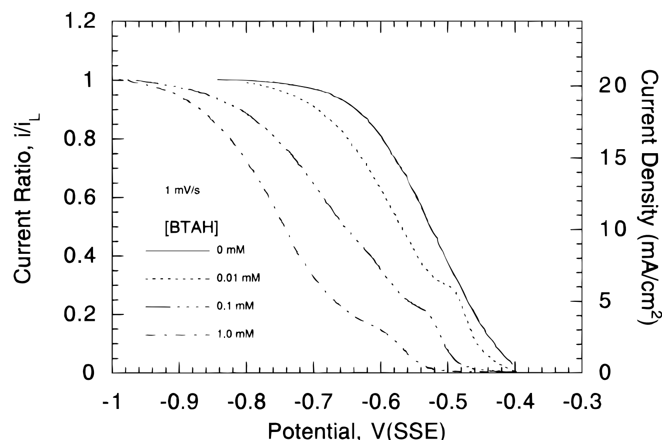

Figure 8. The effect of BTAH concentration on the inhibition of copper deposition. The small wave at low overpotential is absent on the reverse sweep (not shown), but otherwise minimal hysteresis exists in contrast to the i-V curve for the Cl-PEG-MPSA electrolyte.

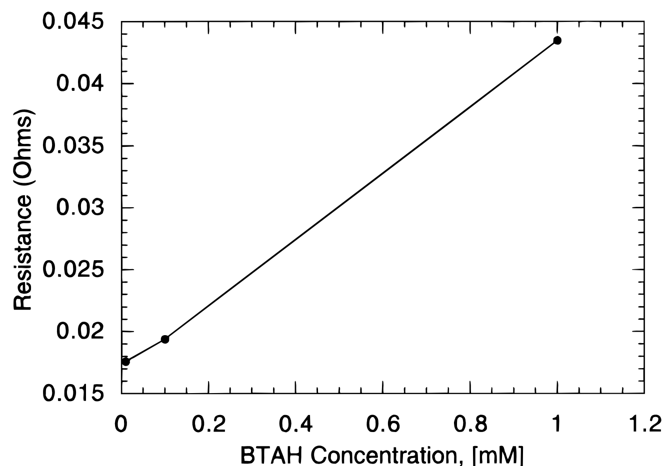

Figure 10. Dependence of film resistance on BTAH concentration.

S0013-4651(00)04-078-7 CCC: $7.00 © The Electrochemical Society, Inc.

that the optical characteristics of the copper were altered. Also, the resistivity was unsuitable for interconnect applications. Nonetheless, the resistance was observed to decrease with a time constant that, nominally, scales inversely with BTAH concentration (not shown). These observations indicate that additive incorporation and grain refinement increase with BTAH concentration, in agreement with previous work.[19]

Damascene pattern plating.—The efficacy of the various additive combinations for superconformal deposition was investigated. As a baseline for these studies, films produced from additive-free electrolyte were also examined.

Additive-free electrolyte.—An FIB image of a cross-sectioned 280 nm thick film deposited at −0.563 V for 45 s from the additive-free electrolyte is shown in Fig. 11. A significant fraction of the cross-sectional area of the low-aspect-ratio trenches are filled, although a circular void is found toward the top center of the wider trenches. In the narrower trenches, with the higher aspect ratios, the voids are elongated, forming a vertical seam that corresponds to ~10% of the trench width, as predicted by simulations.[34] The change in void shape reflects the diminished influence of deposition from the bottom of the trench as the aspect ratio increases. The voids are anticipated from theory due to the depletion of the cupric concentration with trench depth.[34-36] An FIB image that reveals a larger area of the free surface is shown in Fig. 12. In the case of the widest trenches, the film thickness corresponds to the point of void creation or pinch-off at the trench opening. Close inspection of the discontinuous groove reveals intermittent contact between the two sidewalls as a function of distance along the groove. This demonstrates that pinch-off is correlated to some extent with surface roughness.

Figure 11. FIB image of copper deposited from the additive-free electrolyte (−0.563 V for 45 s). Three different groups from the same sample are shown. From left to right the trench width ranges from 370 to 110 nm while the aspect ratio varies from 1.1:1 to 3.8:1. Note that the shape of the void changes from a circle to an elongated seam as the trench becomes narrower. The seam corresponds to ~10% of the trench width as anticipated by published simulations.[34]

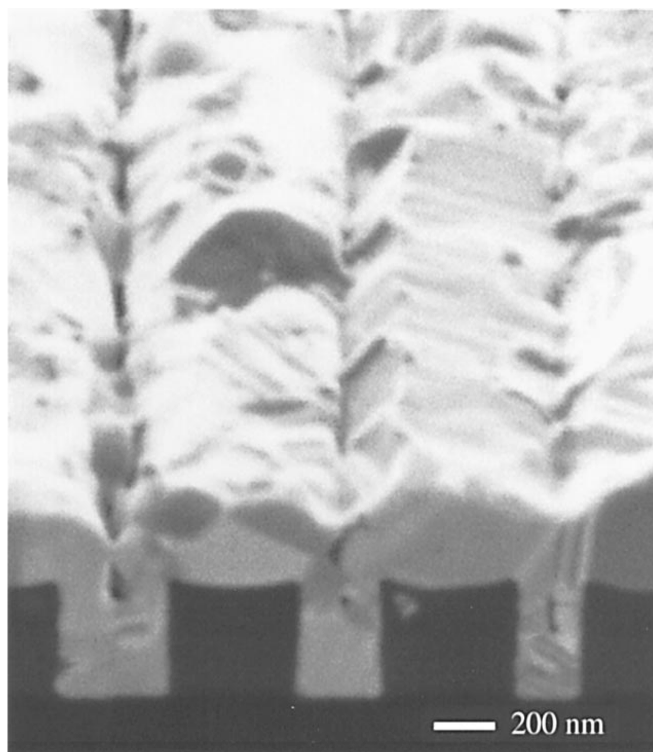

Figure 12. An FIB image showing how void formation due to "pinch-off" is correlated with surface roughness of the colliding sidewalls. Note the intermittent contact or coalescence along the groove demarcating the interface between the colliding sidewalls in the widest trenches. Copper was deposited at −0.563 V for 45 s from the additive-free electrolyte.

In experiments that involved deposition into trenches with slanted sidewalls, typically ~7° from the surface normal, significantly fewer defects were observed (Fig. 13). Three of the six groups of trenches fabricated are shown. The slanted sidewalls are the result of deformation associated with stress development during deposition of the copper seed layer. The outermost trenches of each group were found to be the most heavily distorted. The samples shown in Fig. 13 were deposited at −0.572 V for 60 s, which yielded a nominal film thickness of 550 nm. The sharp groove evident in the 500 nm wide trench is a natural consequence of conformal growth in trenches with slanted sidewalls (in this case as high as 12°). Note that for conformal growth, the center of the trench corresponds to a closure seam, the top of which is marked here by the cusp on the free surface. The increasing width toward the top counterbalances the differential cupric ion concentration that develops within the trench. The effective filling of such trenches is also aided by geometric leveling.[2,37] Nevertheless, occluded voids do still exist in the midsections of some trenches, as highlighted by the arrows in Fig. 13. Repetitive ion milling and imaging revealed that the voids are discontinuous and randomly distributed along the length of the trench. A magnified view of a void in a 250 nm wide trench is shown in Fig. 14. Void formation occurs during the coalescence of the impinging sidewalls. As alluded to earlier, the size and continuity of the voids should correlate to surface roughness of the approaching surfaces. Since roughness typically scales with film thickness, it is anticipated that for a given geometry (aspect ratio and sidewall angle) the void density will decrease with feature size. This is consistent with the fact that no voids were resolved in the higher aspect trenches which have widths less than 200 nm.

Additive electrolytes.—Cl-PEG.—An FIB image of a film deposited at −0.770 V for 45 s from the Cl-PEG electrolyte reveals

S0013-4651(00)04-078-7 CCC: $7.00 © The Electrochemical Society, Inc.

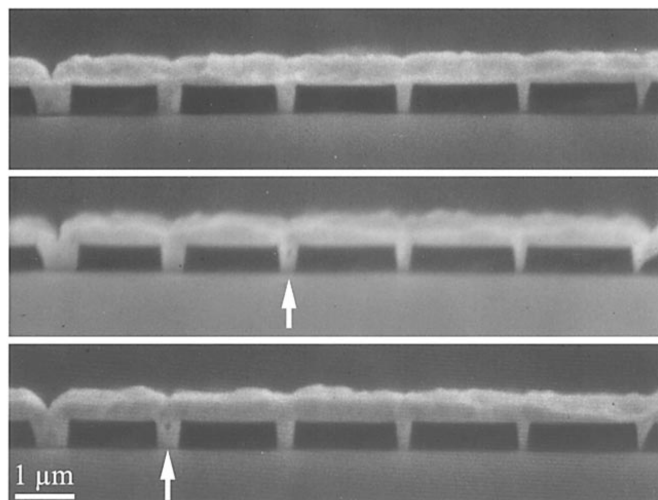

Figure 13. SEM images of copper deposited from an additive-free electrolyte into trenches with slanted sidewalls (−0.570 V for 60 s). Three different groups from the same sample are shown. A selective sampling of the trenches suggests that the sidewalls deviate on the order of 7° from the surface normal. The width at the base of the trenches ranges from 500 to 100 nm and the PMMA template is 500 nm thick. The sharp cusp in the widest trench is a consequence of conformal deposition. White arrows highlight discontinuous voids that randomly appear and disappear with ion milling. No voids were resolved in the narrowest trenches.

large voids in the center of all the trenches, as shown in Fig. 15. The voids are circular in the 380 nm wide trenches and become progressively elongated as the aspect ratio increases with the decreasing trench width. The narrowest lithographic trenches (not shown) contained no electrodeposited copper. This is most probably due to incomplete seed-layer coverage or corrosion. However, it is possible that this is an artifact of the FIB process; as the trenches become narrower and the voids occupy an increasing percentage of the cross-sectional area, the thin copper ligaments along the sidewalls might not be able to withstand the ion bombardment. Evidence in support of this is provided by the bulging and missing sections of the 135 nm trenches. It is noteworthy that the voids are larger than those observed in the absence of additives. The possibility of additives generating larger voids than occur in their absence has been recently explored by simulations.[34] Enhancement of void formation is predicted when the leveling agent is completely consumed at an intermediate position within the trench. The resulting differential inhibition leads to a larger variation in the cupric ion concentration than in the absence of the

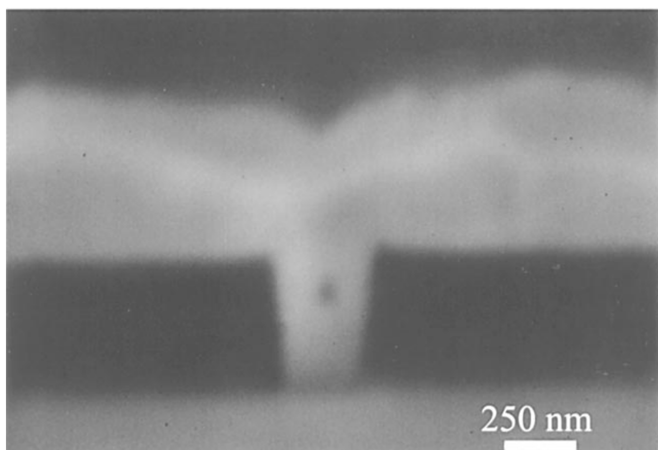

Figure 14. A higher magnification image of a 250 nm trench taken from Fig. 13 exhibiting both a void and significant deviation of the sidewalls from 90°.

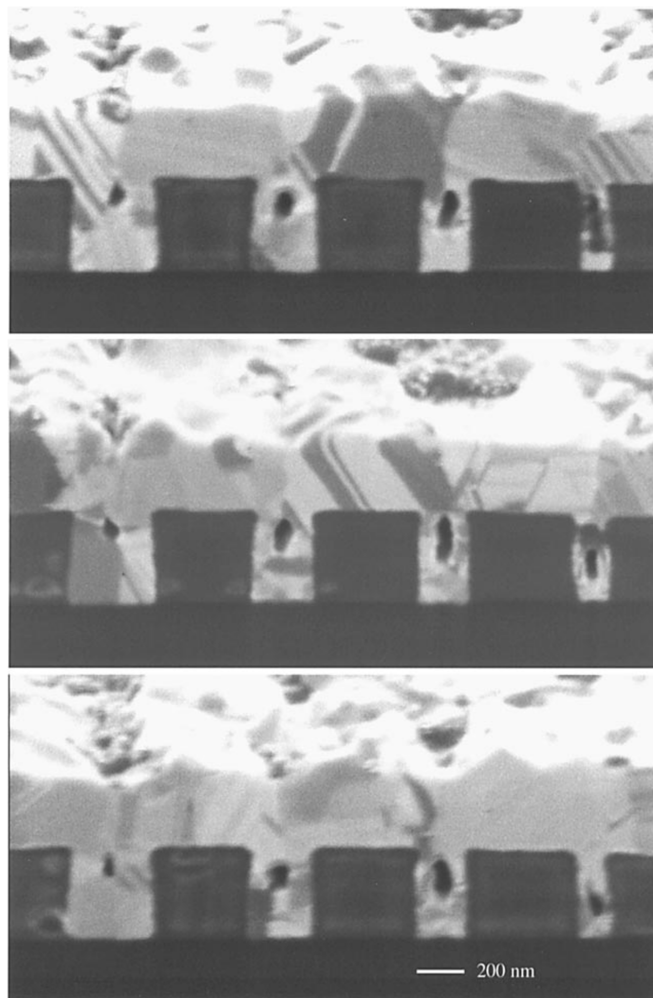

Figure 15. FIB images of copper deposited in three different groups from the Cl-PEG electrolyte (−0.770 V for 45 s). The trench width ranges from 380 to 135 nm with the aspect ratio spanning 1.2:1 to 3.4:1. The large voids that are apparent in all the trenches are notably larger than those found in absence of additives (*i.e.,* Fig. 11).

inhibiting species. In the present system, these observations are difficult to reconcile with the resistivity data that indicate minimal incorporation of the additives, Cl and PEG, within the solid. An alternative possibility is that void "pinch-off" occurs at an earlier time than during deposition from the additive-free electrolyte because of greater surface roughness in the Cl-PEG case, although this needs to be confirmed by roughness measurements.[16]

Cl-MPSA.—A cross section of a specimen deposited at –0.560 V for 45 s from the Cl-MPSA electrolyte reveals continuous voids in all trenches less than 275 nm wide, as shown in Fig. 16. Voids appeared in three (of eight) of each of the larger trenches (in different groups). It is important to note that many of the trenches exhibit a slightly reentrant sidewall angle that is expected to correlate directly to void formation in the case of conformal growth. The large voids, as compared to those observed for the additive-free electrolyte might be, at least partly, ascribed to this.

Cl-PEG-MPSA.—An FIB image of a sample grown at −0.610 V for 45 s in the Cl-PEG-MPSA electrolyte reveals filling of trenches from 350 to 90 nm in width (Fig. 17). Since the seed layer corresponds to 6 nm on each side of the trenches, the narrowest trenches filled by the electrodeposition process corresponds to a width of ~80 nm and an aspect ratio of ~6.6:1. The effective filling despite the slightly reentrant character of the sidewalls is noteworthy, although a sampling of several sections revealed a random distribution of small voids in some

S0013-4651(00)04-078-7 CCC: $7.00 © The Electrochemical Society, Inc.

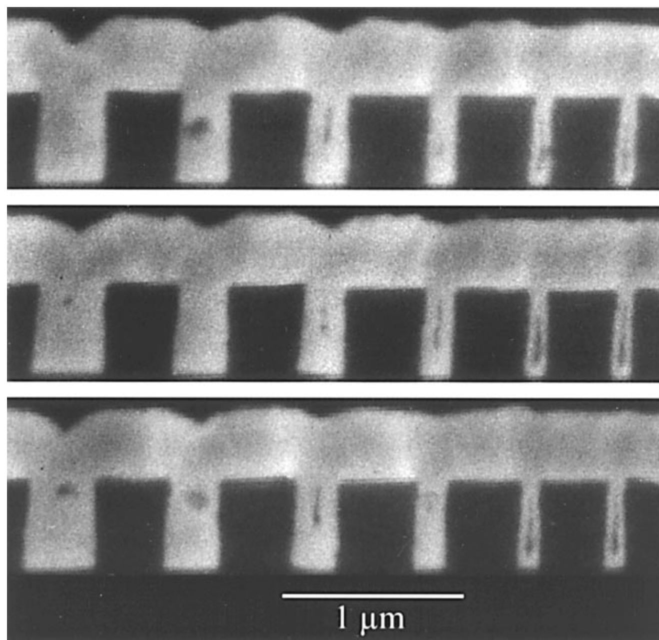

Figure 16. SEM images of copper deposited in three different groups from the Cl-MPSA electrolyte (−0.560 V for 45 s). Small circular voids are apparent in the widest trenches. They become elongated seams as the trench width decreases. Note the voids may be accentuated due to the slightly reentrant sidewall angle.

of the narrowest trenches. The small voids appear and disappear with milling time, indicating that they are discontinuous. The FIB images reveal that the wider trenches are filled by large grains of copper. In some cases a single crystal occupies the entire trench cross section (twins are evident). This characteristic has been reported for several proprietary processes[7,10] and indicates that recrystallization of the deposit has occurred. This was expected because the FIB experiments were performed 5 days after film deposition.

Similar experiments using patterned samples with slanted sidewalls demonstrated complete filling of all the trenches. The film in Fig. 18 was deposited at −0.650 V for 60 s, corresponding to a nominal thickness of 420 nm. The angle of the sidewalls was distributed between ~3 and 8°. No evidence of void formation was apparent. The concave surface profile of the 500 nm wide trenches is distinctly different from the cusp associated with growth in the absence of additives (*i.e.,* Fig. 13.). This profile is in qualitative agreement with the reaction front geometry observed in certain commercial processes.[1,38] It also compares favorably with simulations based on the diffusion and adsorption of additives with either an empirically determined inhibition function[1,38] or a given consumption rate for the leveling agent.[34]

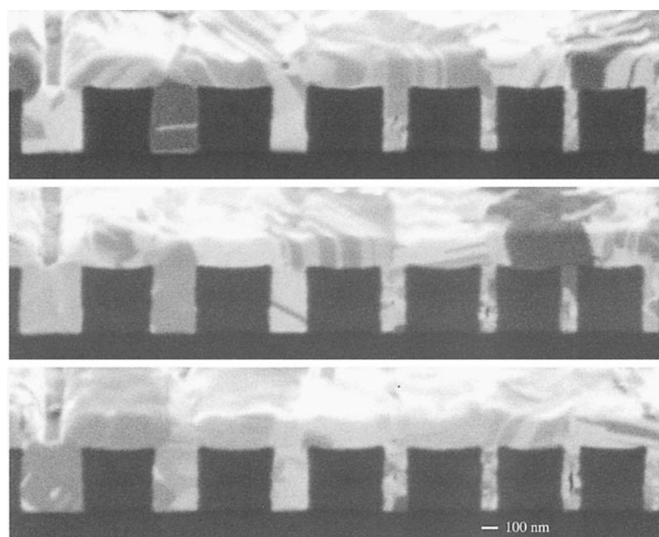

Figure 17. FIB images of copper deposited from the Cl-PEG-MPSA electrolyte into three different groups (−0.610 V for 45 s). The trench width ranges from 350 to 90 nm corresponding to an aspect ratio of 1.5:1 to 5.8:1. No voids were observed in the wider trenches while occasional holes or seams appear randomly distributed in some of the narrower trenches.

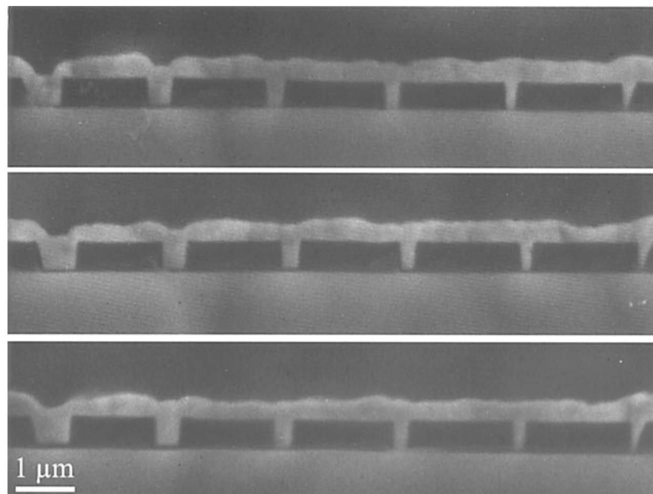

Figure 18. SEM images of copper deposited from the Cl-PEG-MPSA electrolyte into three different trench groups with slanted sidewalls (−0.650 V for 60 s). The width at the base of each trench ranges from ~560 to 120 nm corresponding to an aspect ratio of 0.86:1 to 4.1:1. No voids were observed in any of the trenches. The concave shape of the copper surfaces above the wider trenches is distinctly different from the cusp shape observed in Fig. 13.

Insight into the growth process can be gained by interrupting the deposition process at several times prior to complete filling of the features. Alternatively, one can examine the filling process by studying trenches of different widths for a single deposition time. An example of this is shown in Fig. 19, which was plated at −0.650 V for 30 s. The concave growth front and sharply inhibited deposition at the upper corners of the 300 nm wide trench (Fig. 19a) clearly reflect favored growth from the bottom of the trench. This preferential inhibition is also apparent in surface profiles of the 250 nm wide trenches (Fig. 19b). A residual poisoning effect manifests in the slight inversion of the surface profile in the region above the 200 nm wide trench (Fig. 19c).

In further studies, with vertical or slightly reentrant trenches, inversion or the "overfill" phenomenon was observed. As shown in Fig. 20, bumps become apparent above the trenches as the nominal film thickness increases from 270 (Fig. 20a) to 450 nm (Fig. 20b). These bumps are distinctly different from those associated with the planar surface regions during conformal deposition, *i.e.,* Fig. 16. In the present example the bumps due to "overfill" appear to scale with trench width. Similar effects have been reported for films grown from a range of commercial electrolytes.[4-6] Importantly, this morphology is at odds with the diffusion-limited inhibition model of superconformal deposition and is more consistent with the development of surface regions whose differential reactivity is dependent on history and geometry.

In summary, the Cl-PEG-MPSA electrolyte appears to exhibit the essential characteristics required for superconformal deposition. No attempt was made to optimize the processing parameters for this system.

BTAH.—The efficacy of BTAH toward superconformal deposition was examined in order to explore the possibility of simplifying the process by using an electrolyte with only one additive. Pattern plat-

S0013-4651(00)04-078-7 CCC: $7.00 © The Electrochemical Society, Inc.

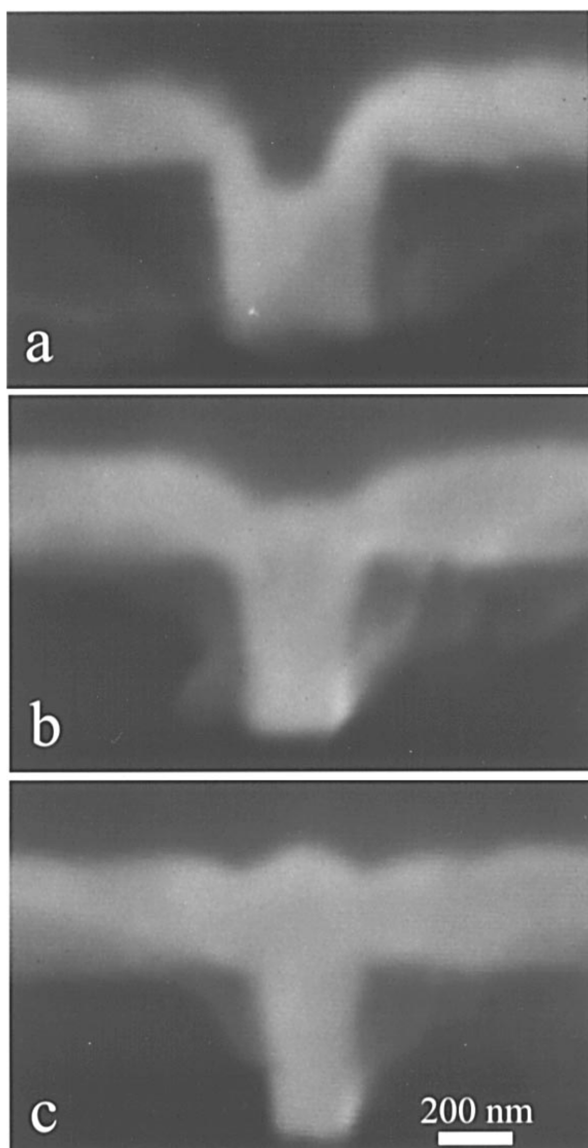

Figure 19. Three SEM images of (a) 300, (b) 250, and (c) 200 nm wide trenches, selected from one specimen, revealing the shape evolution during deposition from the Cl-PEG-MPSA electrolyte (−0.650 V for 30 s). The concave growth surface and the slower deposition at the trench mouth in image (a) reflect the preferential filling from the trench bottom. Likewise, the inversion of curvature apparent in image (c), which is bounded by the parallel grooves, suggests some remnant inhibition associated with growth propagating from the trench corners.

ing was examined for two different BTAH concentrations. As shown in Fig. 21, the sample deposited from 10 μmol/L BTAH solution failed to effectively fill any of the features. The resulting voids were larger than those formed in the absence of additives. This is analogous to the Cl-PEG electrolyte, although the smooth elongated shape of the void seam in the narrower trenches indicates that the growth was more conformal in nature in this instance. Deposition from 100 μmol/L solution at −0.696 V for 20 s also resulted in incomplete filling of the trenches, as shown in Fig. 22. In this case, the voids exhibited a teardrop shape that becomes narrower as the aspect ratio of the trench decreases.

Discussion

The Cl-PEG-MPSA electrolyte yields superconformal copper deposition into trenches between 500 and 90 nm in width with an aspect ratio ranging from 1:1 to ~6.6:1. In related experiments, recrystallization of blanket films deposited from the Cl-PEG-MPSA

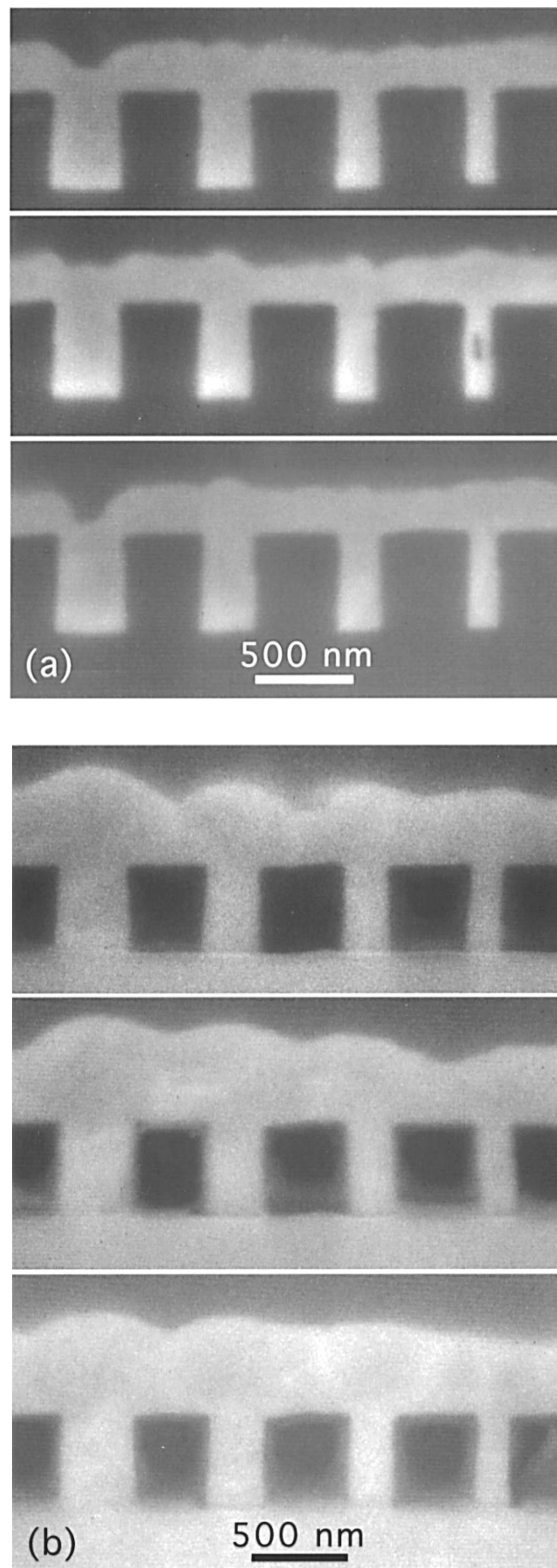

Figure 20. SEM images revealing the "overfill" phenomenon associated with deposition from the Cl-PEG-MPSA electrolyte. The inversion of the surface profile becomes obvious as the nominal film thickness increases from (a) 270 to (b) 450 nm. The films were deposited at −0.687 V for 25 and 45 s, respectively.

S0013-4651(00)04-078-7 CCC: $7.00 © The Electrochemical Society, Inc.

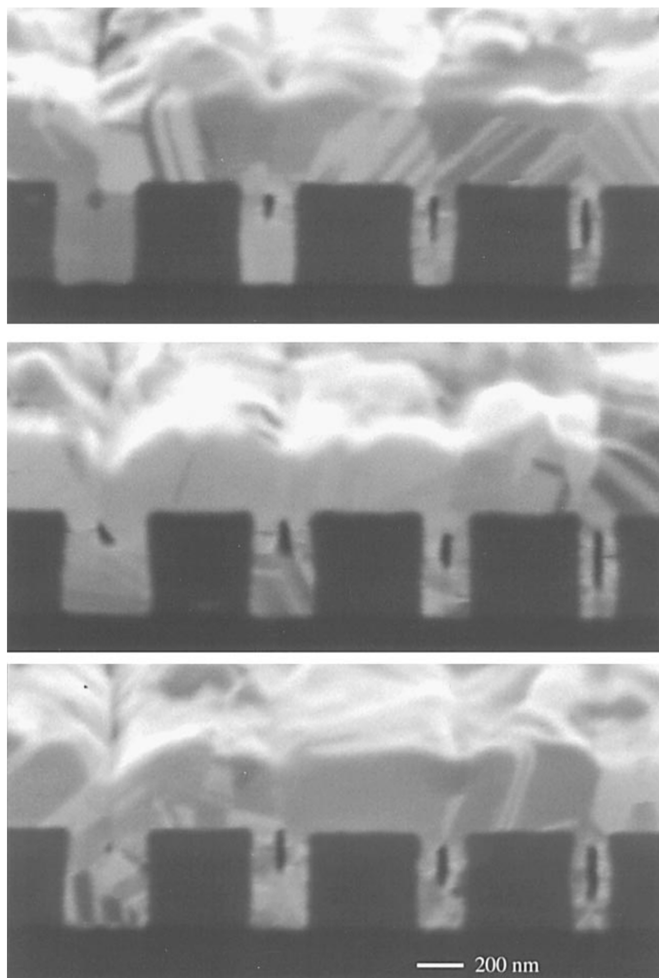

Figure 21. Three FIB images of copper deposited from the 10 μmol/L BTAH electrolyte into three different groups (−0.635 V for 45 s). The trench width ranges from 365 to 150 nm while the aspect ratio varies from 1.4:1 to 3.3:1. Voids are apparent in all the trenches, although the shape is notably different from that observed for samples grown in the Cl-PEG electrolyte (Fig. 15).

electrolyte was observed and found to be consistent with reports for similar films produced by proprietary means.[7,10] This strongly suggests that this system is representative of commercial electrolytes and may be usefully employed as a model or "test bed" for exploring the "superfilling" phenomenon.

Comparison of behaviors of the control samples, Cl-PEG, Cl-MPSA, BTAH, and additive-free electrolytes, to that of the Cl-PEG-MPSA electrolyte unambiguously reveals the synergism that derives from coadsorption and/or competitive adsorption. Interestingly, the Cl-PEG, Cl-MPSA, and BTAH electrolytes result in voids that are larger than those observed in deposits from the additive-free electrolyte. As noted earlier, this outcome was recently predicted by simulations for the situation where the additive(s) is consumed in the trench too rapidly relative to its penetration into the feature by diffusion.[34] Alternatively, large and irregular voids may arise as a consequence of the surface roughness of the colliding sidewalls. The BTAH electrolyte provides an interesting challenge to the modeling community, since the films are reported to be smoother than those produced from additive-free electrolytes[19,21] yet the voids become larger as the BTAH concentration increases. The failure of this system to fill the trenches may reflect limited exploration of parameter space or it may indicate a deeper aspect of the filling phenomenon that requires a more complicated functional relationship between multiple additives than exists in conventional single-inhibitor leveling models. The successful application of an empirically modified inhibition function[1,38] along with the more recent observation of feature "overfill" lends support to the latter interpretation.

i-E hysteresis, recrystallization, and superconformal deposition.—The correlation between the hysteresis observed in the slow-scan *i-E* curve, the recrystallization behavior, and the superconformal deposition for the Cl-PEG-MPSA electrolyte is perhaps the most intriguing result presented in this study. The absence of hysteresis in the case of the additive-free, Cl-PEG, or Cl-MPSA electrolyte demonstrates that the hysteresis is the direct result of alteration in the surface chemistry rather than a physical effect, *e.g.,* a diffusional relaxation associated with scan direction. Thus, the hysteretic response reflects the competition between the rate of metal deposition and the accumulation and consumption of inhibiting additives. From an analytical perspective the slow scan cyclic voltammetric experiments may offer a simple screening tool for the exploration and optimization of new electrolytes. Likewise, they may be useful as a process monitoring tool for assaying "brightener" activity. Although a detailed description of the system response remains to be developed, the measurement itself is a direct reflection of the deposition process as opposed to the widely employed, but somewhat more ambiguous, technique known as cyclic voltammetric stripping analysis (CVS).[39]

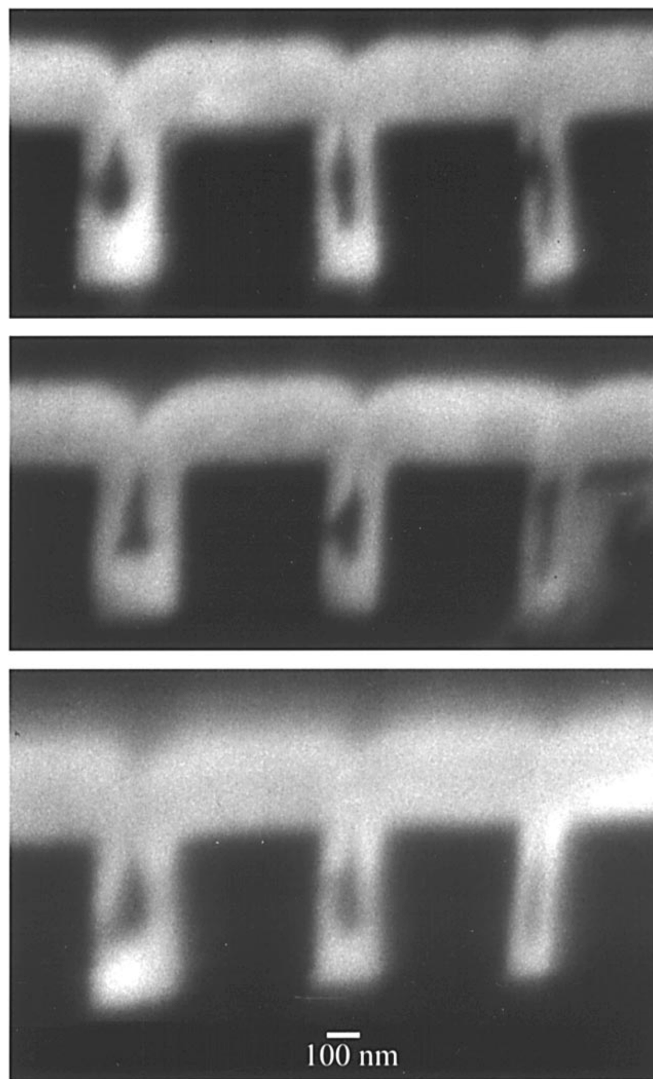

Figure 22. An SEM image of copper deposited from the 100 μmol/L BTAH electrolyte (−0.850 V for 30 s). The trench width ranges from 240 to 140 nm while the aspect ratio varies from 1.9:1 to 3.2:1. Large voids are apparent in all the trenches and the shape is noticeably different from that observed for deposition from the more dilute BTAH electrolyte (Fig. 21).

Journal of The Electrochemical Society, **147** (12) 4524-4535 (2000)
S0013-4651(00)04-078-7 CCC: $7.00 © The Electrochemical Society, Inc.

Hysteresis of *i-E* curves has been predicted for systems where the coverage of the blocking additive is determined by mass transport.[29] No hysteresis is anticipated in the absence of transport control. All the additives examined in this study are known to adsorb on the copper surfaces and exert some influence on the evolution of the surface roughness as gauged qualitatively by the light scattering from the as-deposited surface. The dilute concentration of the MPSA, BTAH, and PEG additions suggests the possibility of transport-controlled adsorption of these species. Likewise, the observation of inhibition increasing with additive concentration (observed for the BTAH electrolyte) is often taken as an indication of diffusion control inhibition. In actuality, this simply indicates the reaction order with respect to the inhibitor concentration. Well-defined and carefully controlled hydrodynamic experiments are required to demonstrate reaction rate control by transport-limited additive adsorption.

In any case, in order to maintain transport control of an inhibitor flux, the adsorbate must either be incorporated in the growing film or reductive desorption must occur during metal deposition. The film resistance measurements are particularly helpful toward assessing the extent of additive incorporation. That the interaction between the constituents of the Cl-PEG-MPSA electrolyte impacts additive incorporation and subsequent structural alteration of the deposits is apparent in Fig. 9. Importantly, this does not occur to a significant extent in the case of the binary systems, Cl-PEG and Cl-MPSA.

A range of reports exists on the surface chemistry between copper and the individual constituents comprising the Cl-PEG-MPSA electrolyte as well as the binary combinations of these additives. Chloride has been stated to be an essential component for the effective operation of cupric sulfate electrolytes.[39-41] It is well established for the bath chemistries studied that the inhibition associated with PEG only occurs in the presence of chloride.[11,12,22-27] Furthermore, the chloride concentration must be kept below $\sim$1 mM in order to avoid precipitation of the CuCl salt.[42] LEED[43] and STM[44,45] studies reveal that chloride is strongly adsorbed on copper single-crystal surfaces, forming ordered structures at potentials typically associated with copper deposition from additive-free electrolytes. At more negative potentials, reductive desorption of chloride occurs with the dynamics of the process being structure sensitive. Other STM studies, in the absence of halide, have revealed ordered sulfate-water adlayers on Cu(111) although no ordered sulfate structures have been reported for the other copper surfaces.[31,46,47] Raman spectroscopy has been used to probe the competitive dynamics between chloride and sulfate adsorption, with chloride adsorption being dominant at potentials associated with copper deposition from additive–free electrolytes.[48] The inhibition provided by PEG might be associated with the formation of a blocking layer on top of the ordered halide layer. It is noteworthy that PEG is known to form complexes with cuprous and chloride ion, both of which participate as intermediates in the deposition reaction.[24] Previously, it has been suggested that the blocking adlayer is a Cu^+Cl-PEG complex[23] that by extension may be specifically adsorbed or linked to the saturated halide adlayer at positive potentials. The subsequent breakdown of this layer at more negative potentials might be due to reduction of the adsorbed complex,[23] or the potential-induced disruption of the underlying chloride layer[43-45] or some combination thereof. The similarity of the resistivities of specimens deposited from the Cl-PEG and additive-free electrolytes indicates minimal incorporation of PEG within the solid. This is in spite of the fact that the surface roughnesses of the blanket films differed significantly.

Limited information is available on the nature of the Cl-MPSA interaction. Prior resistivity measurements[33] for blanket films deposited from a nominally Cl-free MPSA electrolyte resulted in a marked increase in the resistance of the as-deposited film compared to films produced from the Cl-MPSA electrolyte. In related studies, the absence of chloride has been shown to result in significant deterioration of the mechanical properties of copper deposited from electrolytes containing molecules with sulfur-bearing functional groups, *i.e.,* brighteners.[40] These observations are consistent with chloride adsorption competing with the formation of thiolate surface compounds and thereby minimizing the incorporation of sulfur species in the deposit while still being present in a large enough quantity to block epitaxial growth. Simultaneously, both chloride and MPSA are known to form complexes with the cuprous ion reaction intermediate and thus directly impact the reduction mechanism in a manner that is tightly connected with the adsorption dynamics.

In summary, a possible origin of the *i-E* hysteresis effect entails the following sequence of events. Potential-driven desorption or disruption of the blocking Cl-PEG–based layer allows thiolate, or a derivative thereof, to adsorb on the surface. This further disrupts the inhibiting function of the Cl-PEG–based overlayer. The final result is polarization characteristics that tend toward those of the Cl-MPSA electrolyte on the reverse potential sweep. Clearly further work will be necessary to sort out the contribution of the various interactions, especially the connection between additive adsorption and the complex cuprous ion reaction intermediates.

Slanted sidewalls.—Although this paper is primarily concerned with the use of additives to fill well-defined square-wall trenches, experiments with deformed templates revealed a strong influence of slanted sidewalls on the extent of filling. The slanted sidewalls effectively neutralize the influence of the differential cupric ion concentration that develops within the trench; the additional width at the mouth compensates for the higher deposition rate there. Furthermore, the geometric leveling effect[37] also aids the filling of the trenches with slanted sidewalls. These processes appear to be more effective with narrower trenches, which suggests that the roughness of the colliding sidewalls is a key parameter. The latter quantity typically scales with film thickness. In this instance, brighteners that minimize surface roughness might be usefully employed even in the absence of "superfill" dynamics. However, the chemical nature of the impinging surfaces is expected to exert a strong influence on the coalescence occurring at the seam and subsequent microstructural evolution.

Regulation mode.—Filling of trenches is achieved with the potentiostatic conditions employed in this study in spite of the substantial depletion of cupric ion concentration at the interface and the associated relaxation of the concentration gradient. In fact, for the conditions investigated, trenches narrower than 400 nm are completely filled before the steady-state condition is attained. This growth scheme is significantly different from the conventional process where the spatially averaged deposition flux is fixed by galvanostatic regulation. Unfortunately, the high currents associated with the early times of the mixed control potentiostatic transients (*i.e.,* Fig. 3) results in an unfavorable current distribution on the wafer length scale, although this does not appear to impact the question of superfilling being addressed in this report. On the other hand, the firm definition of free energy provided by potentiostatic regulation is helpful as we begin to explore the surface chemistry of the system in more detail.

Conclusions

A model electrolyte containing Cl, PEG, and MPSA additives that generates the two essential characteristics required for successful copper Damascene metallization has been identified. First, superconformal deposition in trenches as narrow as 90 nm with an aspect ratio greater than 5.5:1 has been demonstrated. Second, the fine-grained deposits subsequently undergo recrystallization at room temperature that yields a 23% decrease in resistivity. Films grown from this electrolyte also exhibit the "overfill" phenomenon that is inconsistent with the diffusion-limited inhibition models presented to date. Examination of binary combinations of Cl-PEG-MPSA additives clearly reveals the synergistic nature of the interactions between the three species required for void-free filling of ultralarge-scale integrated (ULSI) features with the desired copper microstructure. The desired attributes appear to correlate with the hysteretic *i-E* response, suggesting its utility as both an investigative screening and process control tool. The polarization and recrystallization behavior of the Cl-PEG-MPSA electrolyte highlights the importance of com-

S0013-4651(00)04-078-7 CCC: $7.00 © The Electrochemical Society, Inc.

petitive and coadsorption effects that deserve further study. Attempts to use electrolytes that exhibit inhibition without hysteresis, such as Cl-PEG and BTAH, result in void formation. Interestingly, the voids are found to be larger than those associated with deposition from additive-free electrolytes.

The National Institute of Standards and Technology assisted in meeting the publication costs of this article.

References

1. P. C. Andricacos, C. Uzoh, J. O. Dukovic, J. Horkans, and H. Deligianni, *IBM J. Res. Develop.,* **42,** 567 (1998).
2. C. Madore, M. Matlosz, and D. Landolt, *J. Electrochem. Soc.,* **143,** 3927 (1996); C. Madore and D. Landolt, *J. Electrochem. Soc.,* **143,** 3936 (1996), and numerous references therein.
3. K. B. Oldham, *J. Electroanal. Chem,* **420,** 53 (1997).
4. J. Reid and S. Mayer, in *Advanced Metallization Conference 1999,* p. 53, M. E. Gross, T. Gessner, N. Kobayashi, and Y. Yasuda, Editors, MRS, Warrendale, PA (2000).
5. T. Ritzdorf, D. Fulton, and L. Chen, in *Advanced Metallization Conference 1999,* p. 101, M. E. Gross, T. Gessner, N. Kobayashi, and Y. Yasuda, Editors, MRS, Warrendale, PA (2000).
6. E. Richard, I. Vervoort, S. H. Brongersma, H. Bender, G. Beyer, R. Palmans, S. Lagrange, and K. Maex, in *Advanced Metallization Conference 1999,* p. 149, M. E. Gross, T. Gessner, N. Kobayashi, and Y. Yasuda, Editors, MRS, Warrendale, PA (2000).
7. J. M. E. Harper, C. Cabral, P. C. Andricacos, L. Gignac, I. C. Noyan, K. P. Rodbell, and C. K. Hu, *J. Appl. Phys.,* **86,** 2516 (1999), and references therein.
8. B. Ke, J. J. Hoekstra, B. C. Sison, and D. Trivich, *J. Electrochem. Soc.,* **106,** 382 (1959).
9. V. A. Lamb, C. E. Johnson, and D. R. Valentine, *J. Electrochem. Soc.,* **117,** 291C (1970), *J. Electrochem. Soc.,* **117,** 291C, 341C, 381C (1970).
10. C. Lingk and M. E. Gross, *J. Appl. Phys.,* **84,** 5547 (1998), and references therein.
11. M. Goodenough and K. J. Whitelaw, *Trans. Inst. Met. Fin.,* **67,** 57 (1989).
12. J. P. Healy, D. Pletcher, and M. Goodenough, *J. Electroanal. Chem.,* **338,** 155 (1992).
13. J. P. Healy, D. Pletcher, and M. Goodenough, *J. Electroanal. Chem.,* **338,** 167 (1992).
14. J. P. Healy, D. Pletcher, and M. Goodenough, *J. Electroanal. Chem.,* **338,** 179 (1992).
15. M. Wuensche, W. Dahms, H. Meyer, and R. Schumacher, *Electrochim. Acta,* **39,** 1133 (1994).
16. J. J. Kelly and A. C. West, *Electrochem. Solid-State Lett.,* **2,** 561 (1999).
17. H-G. Creutz, R. M. Stevenson, and E. A. Romanowski, U.S. Pat. 3,267,010 (1966); 3,288,690 (1966).
18. D. Tromans and R. Sun, *J. Electrochem. Soc.,* **138,** 3235 (1991).
19. J. K. Prall and L. L. Shreir, *Trans. Inst. Met. Fin.,* **41,** 29 (1964).
20. E. E. Farndon, F. C. Walsh, and S. A. Campbell, *J. Appl. Electrochem.*, **25,** 574 (1995).
21. R. M. Rynders and R. C. Alkire, *J. Electrochem. Soc.,* **141,** 1166 (1994).
22. M. R. H. Hill and G. T. Rogers, *J. Electroanal. Chem.,* **86,** 179 (1978).
23. M. Yokoi, S. Konishi, and T. Hayashi, *Denki Kagaku,* **52,** 218 (1984).
24. D. Stoychev and C. Tsvetanov, *J. Appl. Electrochem.,* **26,** 741 (1996).
25. J. D. Reid and A. P. David, *Plat. Surf. Fin.,* 66 (Jan 1987).
26. J. J. Kelly and A. C. West, *J. Electrochem. Soc.,* **145,** 3472 (1998).
27. J. J. Kelly and A. C. West, *J. Electrochem. Soc.,* **145,** 3477 (1998).
28. C. R. Wilke, M. Eisenberg, and C. W. Tobias, *J. Electrochem. Soc.,* **100,** 513 (1953).
29. D. Roha and U. Landau, *J. Electrochem. Soc.,* **137,** 824 (1990).
30. M. R. Vogt, W. Polewska, O. M. Magnussen, and R. J. Behm, *J. Electrochem. Soc.,* **144,** L113 (1997).
31. W. Polewska, M. R. Vogt, O. M. Magnussen, and R. J. Behm, *J. Phys. Chem. B,* **103,** 10440 (1999).
32. H. Y. H. Chan and M. J. Weaver, *Langmuir,* **15,** 3348 (1999).
33. G. R. Stafford, M. D. Vaudin, T. P. Moffat, N. Armstrong, and D. R. Kelly, in *Advanced Metallization Conference 1999,* p. 53, M. E. Gross, T. Gessner, N. Kobayashi, and Y. Yasuda, Editors, MRS, Warrendale, PA (2000).
34. A. C. West, *J. Electrochem. Soc.,* **147,** 227 (2000).
35. A. C. West, C. C. Cheng, and B. C. Baker, *J. Electrochem. Soc.,* **145,** 3070 (1998).
36. K. M. Takahashi and M. E. Gross, *J. Electrochem. Soc.,* **146,** 4499 (1999).
37. O. Kardos and D. Gardner, in *Advances in Electrochemistry and Electrochemical Engineering,* P. Delahey and C. W. Tobias, Editors, Vol. 2, p. 145, John Wiley & Sons, Inc., New York (1962).
38. H. Deligianni, J. O. Dukovic, P. C. Andricacos, and E. G. Walton , in *Electrochemical Processing in ULSI Fabrication and Semiconductor/Metal Deposition II,* P. C. Andricacos, P. C. Searson, C. Reidsema-Simposon, P. Allongue, J. L. Stickney, and G. M. Oleszek, Editors, PV 99-9, p. 52, The Electrochemical Society Proceedings Series, Pennington, NJ (1999).
39. D. Tench and J. White, *J. Electrochem. Soc,* **132,** 831 (1985); R. Haak, C. Ogden, and D. Tench, *Plat. Surf. Fin.,* **52,** (April 1981).
40. D. Anderson, R. Haak, C. Ogden, D. Tench, and J. White, *J. Appl. Electrochem.,* **15,** 631 (1985).
41. S. Yoon, M. Schwartz, and K. Nobe, *Plat. Surf. Fin.,* 65, (Dec 1994).
42. T. Kekesi and M. Isshiki, *J. Appl. Electrochem.,* **27,** 982 (1997).
43. C. B. Ehlers, I. Villegas, and J. L. Stickney, *J. Electroanal. Chem.,* **284,** 403 (1990).
44. T. P. Moffat, *Mater. Res. Soc. Symp. Proc.,* **404,** 3 (1996); T. P. Moffat, in *Electrochemical Processing in ULSI Fabrication and Semiconductor/Metal Deposition II,* P. C. Andricacos, P. C. Searson, C. Reidsema-Simpson, P. Allongue, J. L. Stickney, and G. M. Oleszek, Editors, PV 99-9, p. 41, The Electrochemical Society, Pennington, NJ (1999).
45. M. R. Vogt, F. Moller, C. M. Schilz, O. M. Magnussen, and R. J. Behm, *Surf. Sci.,* **367,** L33 (1996).
46. M. Wilms, P. Broekmann, C. Stuhlmann, and K. Wandelt, *Surf. Sci.,* **416,** 121 (1998).
47. W. Li and R. J. Nichols, *J. Electroanal. Chem.,* **456,** 153 (1998).
48. G. M. Brown and G. A. Hope, *J. Electroanal. Chem.,* **405,** 211 (1996).